



Novel Control Strategy for CESS Integrated DC Microgrid with On Grid and Off Grid Application

Ramjee Lal Meena¹ · Avik Bhattacharya² · Dheeraj K. Khatod²

Received: 16 July 2022 / Accepted: 20 February 2023 / Published online: 10 April 2023
© King Fahd University of Petroleum & Minerals 2023

Abstract

Due to increasing role of DC generation, such as solar photovoltaic, fuel cells, numerous DC loads, addition of different energy storage systems, such as batteries and supercapacitors, DC microgrid is gaining more importance. Distributed generators, electronically controlled loads and composite energy storage systems make the system complex to control the DC bus voltage as constant. A Novel control strategy for CESS integrated DC Microgrid with On grid and Off Grid Applications is proposed for various modes of operation decided by existing conditions. First, utility grid mode is investigated for normal operation and grid side open circuit fault with supercapacitor and without supercapacitor. DC bus voltage, power flow control, real and reactive power control of three-phase nonlinear load is carried out by grid interface converter. Second, PV mode, when grid as well as battery are not able to control DC bus voltage, PV connected boost converter operation has to shift from MPPT to constant voltage control mode in coordination of supercapacitor. In combined control of PV and supercapacitor, later is mitigating the DC bus voltage ripple and stability problem due to constant power load. Third, energy storage mode, battery and super capacitor control the DC bus voltage by combined control strategy. Battery handles the energy density component, whereas supercapacitor power density. The Proposed scheme is simulated in MATLAB/SIMULINK environment for steady state and various transient/disturbance conditions and the corresponding operation, control and stability aspects are analyzed. The simulation results are verified with the help of Hardware-In-Loop (HIL) OPAL-RT (RT-4210) simulator.

Keywords Solar photovoltaic · Composite energy storage system · Constant power load · Nonlinear load · DC Microgrid · Opal-RT lab

1 Introduction

Due to gradual depletion of fossil fuel resources, poor energy efficiency and environmental pollution, conventional fossil-fueled power generation systems are being paid less attention [1]. To meet increasing demand of per capita power consumption, a new trend of generating power locally at distribution voltage level is emerging. This type of power generation

is termed as distributed generation (DG) [2]. Distributed generation can utilize both small-scale conventional energy generation technologies like gas and micro-turbines and non-conventional renewable energy generation technologies like solar photo-voltaic (SPV) panels, wind turbines (WTs), fuel cells (FCs), etc.[2, 3]. The integration of renewable energy sources offers several challenges due to their intermittent output and hence requires an energy storage system to enable time-shift between energy production and consumption [4, 5].

Microgrid (MG) is defined as a cluster of AC-DC sources, distributed storage devices and distributed loads that operate in a controlled manner so as to improve the reliability and quality of the local power supply and of the power system as a whole. Based on their network topologies microgrids are classified as AC, DC and hybrid microgrid [6, 7]. Many renewable energy sources like SPV and FC generate low-voltage DC power. Most of the sources supply power to AC grid to multiple AC to DC conversion posing

✉ Ramjee Lal Meena
meenarl@yahoo.com

Avik Bhattacharya
avik.iitkqp@gmail.com

Dheeraj K. Khatod
dheerfee@iitr.ac.in

¹ Department Hydro and Renewable Energy, IIT Roorkee, Roorkee 247667, India

² Department of Electrical Engineering, IIT Roorkee, Roorkee 247667, India



the problem of power quality and overall efficiency of the grid [8]. The introspective review of the ACMG and DCMG with renewable-based DG units, energy storage devices and loads is presented in detail [9]. However, power transmission through a low-voltage DC link produces more losses than transmission through a high-voltage AC link. With development of microgrid control methods along with cost-effective and efficient power converters, a DC link micro-grid can become a promising solution for integrating DG sources, storages and loads [10]

1.1 Literature Review

In DCMG multiple sources, storages and loads are to be integrated and operated in controlled, stable and reliable manner [10, 11]. This is achieved by providing interfacing with the help of power electronics converters feed with by various control strategies [12, 13]. Microgrid applies coordinated control to achieve voltage regulation, power sharing, mode of operations and energy management among various component of microgrid including interaction with utility grid. Based on communication channel used, the coordinated control is classified as centralized, decentralized and distributed control. Hierarchy of control is another division of control strategies e.g., primary, secondary and tertiary level based on functionalities [10, 14]. An autonomous control method for a DCMG having distribution generation, storage and connected utility grid is investigated in [15]. This control method detects only the dc grid voltage resulting in suppression of circulating current.

Dynamic power management for PV-fuel cell-based hybrid microgrid with HESS is investigated using moving average filter technique in [16] whereas dynamic energy management is in [17]. Control and operation of a DCMG with intermittent generation and variable energy storage are examined in [18] and power flow control of a CESS standalone PV system under irradiance and load variations is given [19]. DC bus voltage control for PV sources in a DCMG is discussed in [13], the voltage boost operation with variable PV source voltage, is achieved with PI-tuned current and voltage controller for constant bus voltage. Distributed cooperative control of DCMG that derives a global dynamic model and design guidelines to improve tuning for better dynamic response is presented in [14]. DC voltage regulation using new HESS control strategy is reported that makes DCMG sustainable against RES fluctuations in [20]. In [21], design and small signal analysis of DCMG with HESS is investigated. Decentralized control scheme is investigated with RT-LAB simulator under source disturbances for a grid-connected DCMG in [22]. Voltage deviation is used to improve voltage regulation and stability in a islanded DCMG with HESS [23] and dynamic energy management issues for grid-connected DCMG are addressed in [24]

In DCMG distributed power architectures in which point-of-load converters behave as instantaneous constant-power loads (CPLs) to line regulating converters located upstream [25, 26]. These loads introduce transient instability in dc microgrids that may cause their main bus voltages to show significant oscillations or to collapse. Various solutions for this transient instability problem are proposed in [27–29]. However, very less work is reported on combined control on energy density storage and power density storage. Moreover, very little amount of work is reported on combined control of DG with power density storage to reduce DC bus voltage ripple and improve stability. The investigation on impact of power density storage on utility grid and DCMG when AC side fault takes place is also not explored in the literature. Very less work is reported in the literature for fault in utility grid and managed by supercapacitor connected at DC bus. Less attention paid for stability issue when a CPL fed by upper stream DC-DC boost converter which has inherent stability problem due to its right hand side zero.

In this paper, a novel coordinated distributed control strategy among various sources, loads, storages and utility grid is proposed. The proposed flexible and reliable DCMG can operate On grid, Off grid and with battery or without battery/supercapacitor. This supplies power to critical load, constant power load and three-phase nonlinear load. Supercapacitor with its associated combined control strategy that changes its controller association with another converter controller based on mode of operation. A robust stabilize technique is developed for CPL fed by PV boost converter separately for sake of clarity. MATLAB/Simulink results are analyzed and discussed for different operational conditions. These results are validated on OPAL-RT (OP4510) real-time simulator.

The remaining paper is organized in the following sections. In Sect. 2, the proposed grid-connected DCMG architecture and operation are described. The CESS-based proposed control strategy and its implementation is explained in Sect. 3. In Sect. 4, DC-DC boost converter feeding constant power load, stability analysis and mitigation are presented. The results and discussion of developed control strategy are in Sect. 5. Finally, Sect. 6 summarizes the work with conclusion.

2 Grid-Connected DCMG Architecture and Operation

The proposed grid-connected DCMG in this paper is shown in Fig. 1 as a single line diagram (SLD). The DCMG comprised of grid side converter (GSC) i.e., three-phase three-level neutral point clamped (NPC) converter, solar photo-voltaic (SPV), battery and supercapacitor as a composite energy storage system (CESS), DC critical load, constant

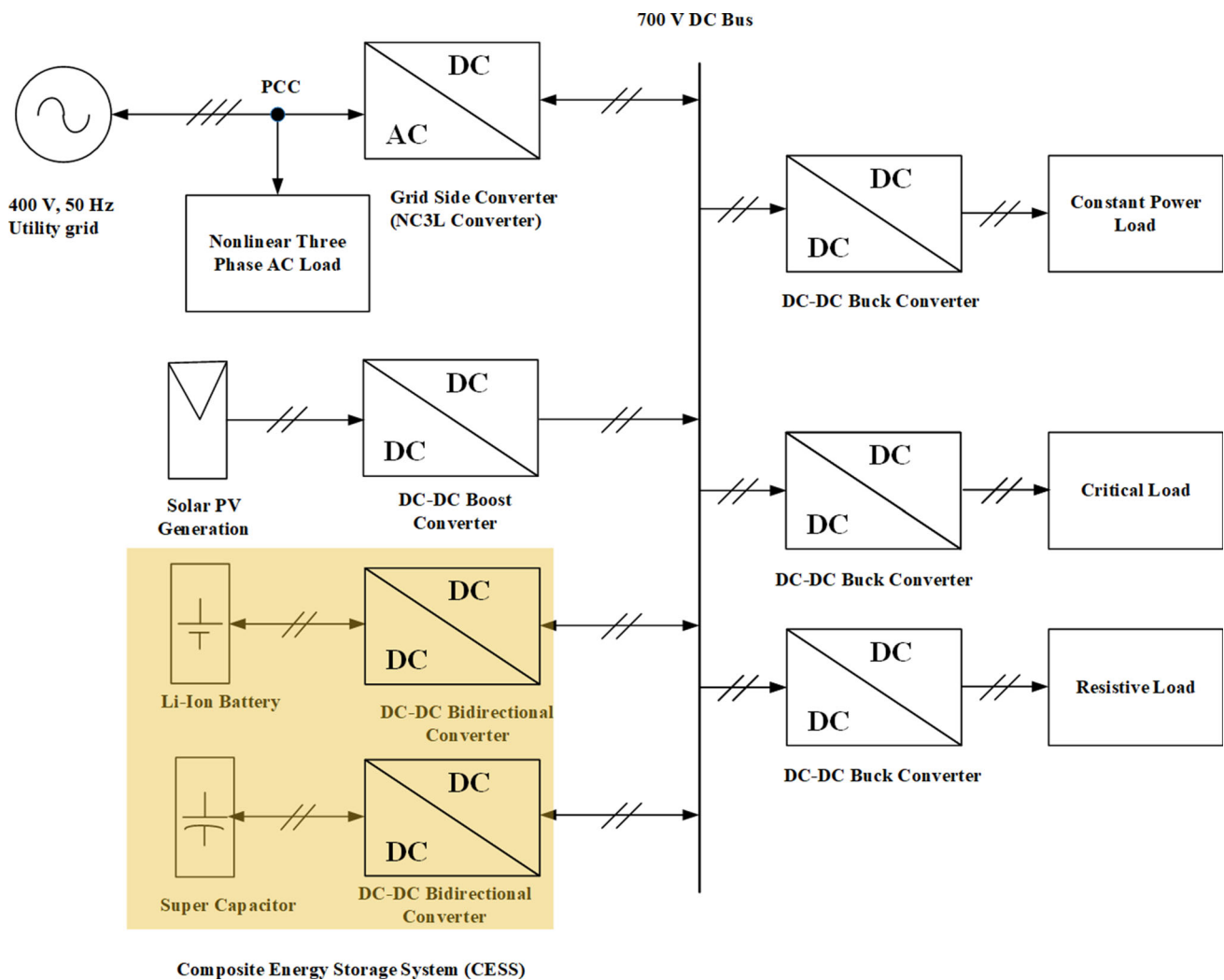


Fig. 1 Single line diagram of proposed grid-connected DCMG

power load (CPL) and three-phase nonlinear load. Utility grid, GSC and nonlinear three-phase load are connected at point of common coupling (PCC). Slanting parallel lines on SLD represent number of conductors and arrow on SLD line indicate direction of flow of power. The interfacing among utility grid, three-phase nonlinear load and DC bus is through GSC. This converter is operated in voltage source converter in current control mode to insure bidirectional flow of power at low THD and unity power factor.

The SPV is connected to DC bus via the DC-DC boost converter. Intermittent DC voltage generated by the SPV is fed to the DC-DC boost converter. DC-DC boost converter perform two functions, (i) track maximum power from PV with changing input conditions and (ii) boost the generated voltage to the DC bus voltage. The maximum power point tracking (MPPT) scheme implemented here is perturb and observe (P&O) algorithm. If a situation of surplus power

arises, MPPT control scheme is replaced with constant voltage control to maintain the bus voltage at rated value.

Composite energy storage system (CESS) is utilized in the proposed grid-connected DCMG. Li-ion battery works as a high energy density storage device. This stores the energy during excess power generation. The stored energy is used to feed the power deficiency. This is connected to the DC bus via bidirectional DC-DC converter. The bidirectional DC-DC converter is controlled by double loop control (outer voltage control loop and inner inductor current control loop) strategy for charging/discharging and bus voltage regulation purpose. Supercapacitor as a power density storage device handles the transient energy fluctuations to achieve bus voltage variations/ripple low. These fluctuations may be caused either by source side disturbances or by load side disturbances or a combined of both. In this paper, combined controller for both storages is proposed.

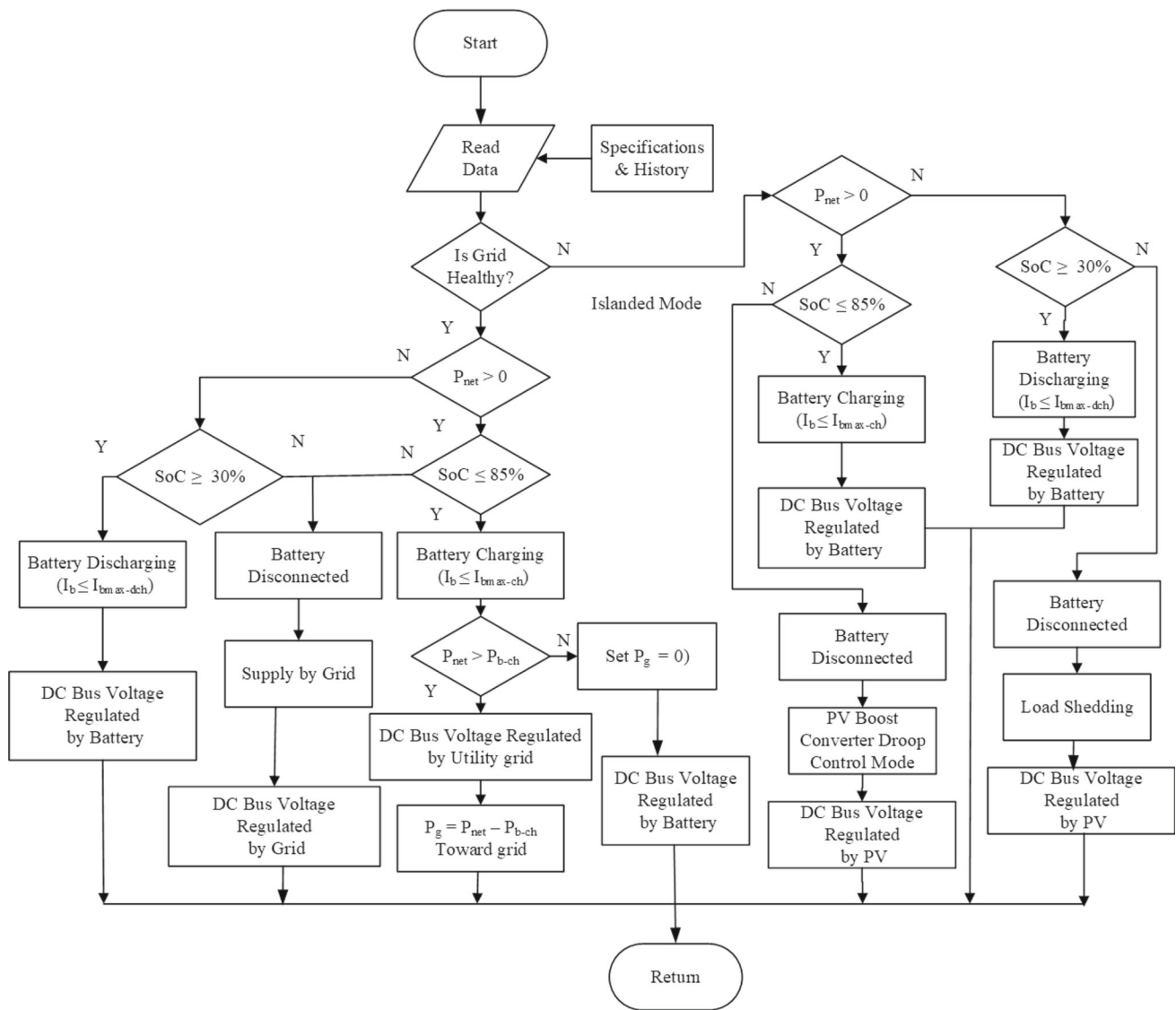


Fig. 2 Operation strategy of proposed DCMG

The proposed grid-connected DCMG operates in three modes as per varying conditions. The operation modes are decided as per the strategy depicted in Fig. 2 of the flow chart. There are three main issues to be addressed during operation; (i) harnessing maximum SPV power generation, (ii) effective use of energy storage system, and (iii) proper regulation of DC bus voltage. These are interrelated control issues.

The distributed control method based on mutual communication among various converters is employed to control power flow and regulate DC bus voltage of the DCMG under varying input/output circumstances as explained in the flow chart [10]. The difference between the generated power by SPV and load demand on DC bus decides the mode of operation of the proposed DCMG, this power difference is denoted by P_{net} in flowchart. Three modes of operation are considered

in this paper based on deciding circumstances/conditions as shown in Fig. 3 [30]. These are discussed below in detail.

2.1 Power Surplus Mode

In this mode, DCMG is not connected with utility grid, it is also known as islanded mode. This mode of operation is shown in Fig. 3a. During this mode, battery is either fully charged or maximum charging rate has been attained. The total demand of load and battery charging power is less than SPV generation. This excessive power in DCMG causes the DC bus voltage to increase beyond the maximum limit. The SPV DC-DC boost converter shifts from MPPT control to constant voltage control to regulate DC bus voltage. Super

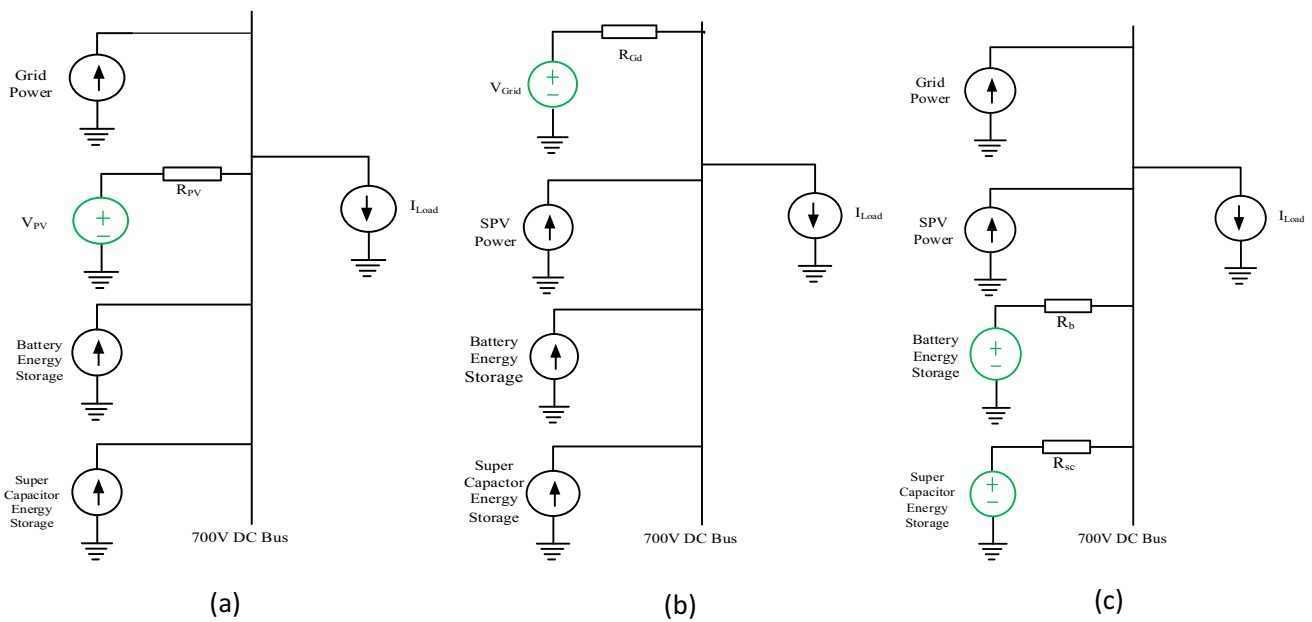


Fig. 3 Grid-connected DCMG operating modes: a power surplus mode, b grid-connected mode, and c CESS mode [30]

capacitor handles the short time variation in DC bus voltage by coordinated controller.

2.2 Grid-Connected Mode

In this mode, circumstances favor the interconnection between utility grid and DCMG, when SPV is not able to meet load demand, grid supplied deficit power and control DC bus voltage. This operating mode is shown in Fig. 3b. The SPV converter operates at MPPT control during this mode. The battery may be charging, discharging or in idle mode depending on present SoC, utility energy cost at particular time and future load demand. In this mode, the short time variation in DC bus voltage is handled by super capacitor. In case of power excess in DCMG, it can be absorbed by utility grid in similar manner.

2.3 CESS Mode

This operating mode is shown in Fig. 3c. In this mode load power demand is more/less than SPV generation and utility grid is not connected to compensate the deficit power. Remaining option to supply/absorb deficit/excess power and control DC bus voltage is only CESS. Mainly battery will deal to low frequency power component and manage DC bus voltage within range. In this mode, SPV works on MPPT control. Supercapacitor manage the transient and high frequency power component e.g., CPL.

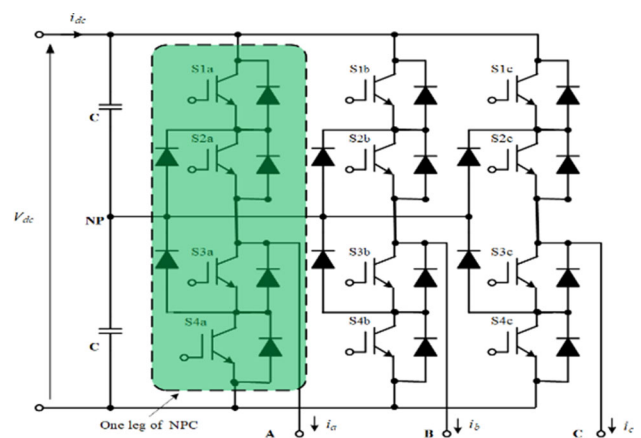


Fig. 4 Three-phase three-level neutral point clamped converter

3 CESS-Based Proposed Control Strategy and Implementation

3.1 Control of Grid Side Converter

In this paper, three-phase three-level neutral point clamped (NPC) converter, as depicted in Fig. 4. is used as an interface between utility grid and DCMG along with three-phase nonlinear load at point of common coupling (PCC) [31]. The control scheme of GSC along with utility grid, DCMG and nonlinear three-phase load is portrayed in Fig. 5. R_L and L_L represent the line resistance and inductance between PCC voltage (V_{PCC}) and utility grid voltage (V_s), respectively. V_{sabc} and i_{sabc} are three-phase grid voltage and current, respectively. The capacitance C_{dc} is employed to regulate

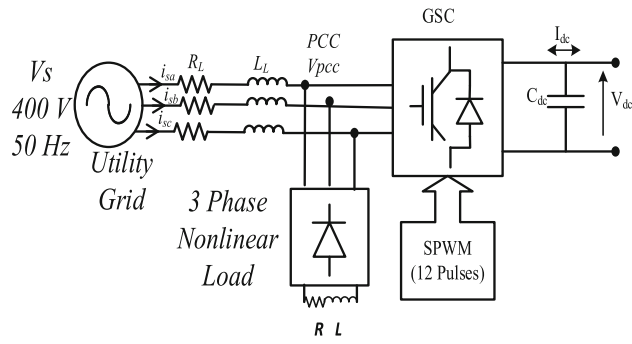


Fig. 5 Utility grid and DC bus interface via three-phase three-level NPC converter

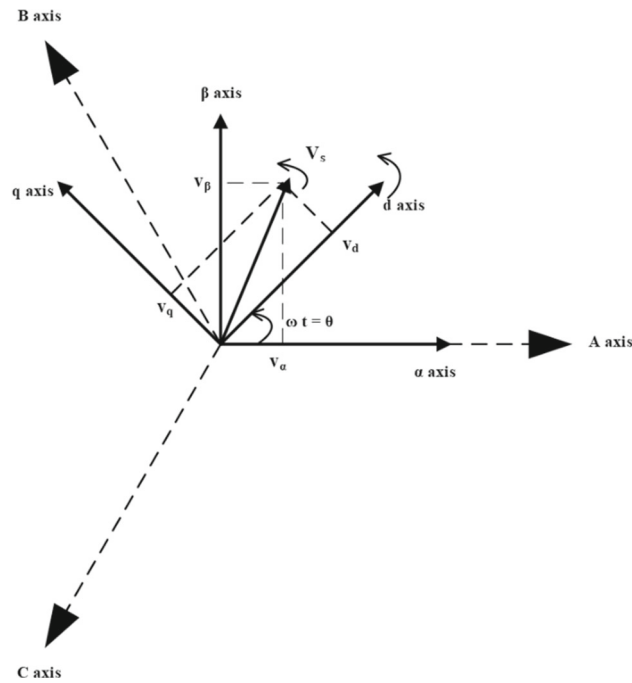


Fig. 6 Synchronous Rotating Frame (SRF)

DC bus voltage (V_{dc}) ripple. When a GSC is integrated with SPV to form a common DC bus, problems on AC side such as voltage unbalance, frequency variations and sag/swell may exist. Three-phase nonlinear load connected at PCC also creates problem related to poor power factor and harmonics. To overcome the above-mentioned problems, two main control schemes are employed collectively, namely phase-locked loop (PLL) and sine pulse width modulation SPWM [22].

PLL detects zero crossing of three-phase voltage and calculate phase angle (ωt). For a balanced three-phase AC supply given in Eq. (1), a synchronous rotating frame (SRF) is depicted in Fig. 6 [32] [33]. PLL control method is developed based on the following mathematical Eqs. (1) to (5)

based on Park’s abc to dqo transformation:

$$\begin{bmatrix} V_{sa} \\ V_{sb} \\ V_{sc} \end{bmatrix} = V_m \begin{bmatrix} \sin(\theta) \\ \sin(\theta - 120^\circ) \\ \sin(\theta + 120^\circ) \end{bmatrix} \quad (1)$$

$$\begin{bmatrix} V_\alpha \\ V_\beta \end{bmatrix} = \begin{bmatrix} V_{sa} \\ \frac{1}{\sqrt{3}}(V_{sc} - V_{sb}) \end{bmatrix} \quad (2)$$

Here θ is angle between a-axis and d-axis as shown in Fig. 6. and θ^* is reference angle for control. In rectification mode of operation, the grid voltage vector \vec{V}_s is aligned with q-axis and the d-axis lags the q-axis by 90° [34].

$$\begin{bmatrix} V_{sq} \\ V_{sd} \end{bmatrix} = \begin{bmatrix} -\sin(\theta^*) & \cos(\theta^*) \\ \cos(\theta^*) & \sin(\theta^*) \end{bmatrix} \begin{bmatrix} V_\alpha \\ V_\beta \end{bmatrix} \quad (3)$$

$$\begin{bmatrix} V_{sq} \\ V_{sd} \end{bmatrix} = V_m \begin{bmatrix} \cos(\theta^* - \theta) \\ \sin(\theta^* - \theta) \end{bmatrix} = V_m \begin{bmatrix} \cos(\Delta\theta) \\ \sin(\Delta\theta) \end{bmatrix} \quad (4)$$

$$\begin{bmatrix} i_{sd} \\ i_{sq} \end{bmatrix} = I_m \begin{bmatrix} \cos(\theta^* - \theta) \\ \sin(\theta^* - \theta) \end{bmatrix} = I_m \begin{bmatrix} \cos(\Delta\theta) \\ \sin(\Delta\theta) \end{bmatrix} \quad (5)$$

To achieve unity power factor operation i_{sq} is set to be zero in control block. i_{dcref} is generated to control the DC bus voltage, I_{gdref} and i_{nl} is reference current corresponding to the power exchange between utility grid and DCMG, and nonlinear load power, respectively as shown in Fig. 7.

3.2 Control of SPV Boost DC-DC Converter

There are two different approaches of control of boost converter which is placed between dc bus and SPV generator. As explained in flowchart in Fig. 2, if sum of power demand by loads, storage and utility grid is more than SPV generation, mode selection switch enables MPPT controller to control the boost converter. While in case of surplus power generation is taking place in MPPT control, this led to increase in the DC bus voltage. To avoid this, MPPT control is required to be shifted to constant voltage control mode by mode selection switch. In Fig. 8, MPPT control, constant voltage control and mode selection switch are explained. Double loop control in coordination with supercapacitor controller is employed for constant voltage control. V_{pv} , I_{pv} and V_{ppref} are voltage, current and MPPT voltage reference of PV generation, respectively. PI controller is employed for all section of control.

To control the DC bus voltage by SPV connected boost converter, the inner current loop and outer voltage loop along with low pass filter (LPF) and rate limiter (RLT) are main part of controller. The ripple voltage generated by subtractor of

Fig. 7 PLL and SPWM control scheme for grid side converter

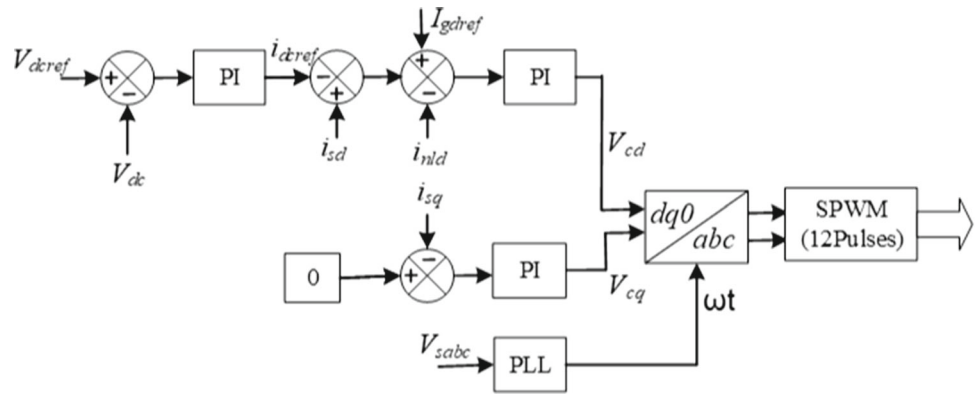
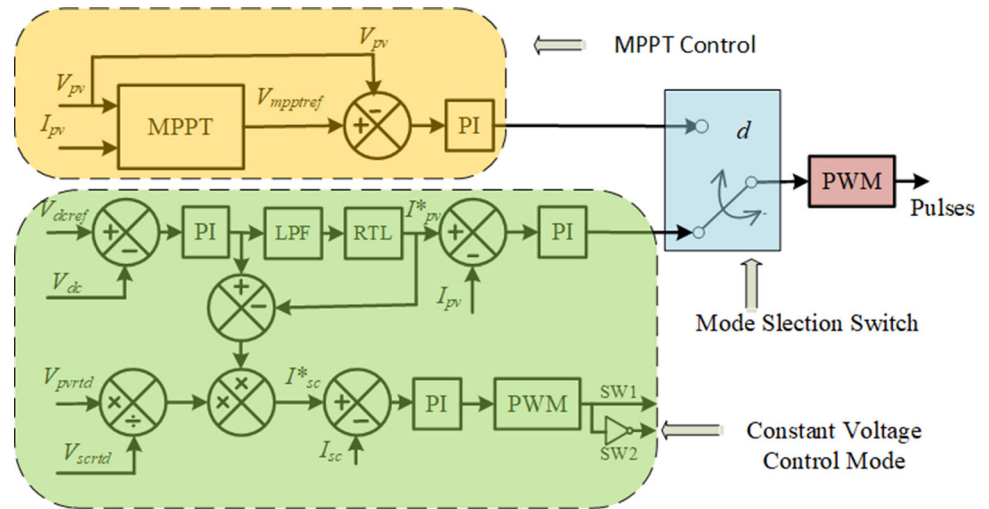


Fig. 8 Control scheme for SPV interfacing boost converter



low pass filter with actual one is considered as a reference for the supercapacitor. $V_{dc\text{ref}}$ and V_{dc} are reference and measured DC bus voltage, respectively. I_{pv}^* and I_{pv} are reference and measured PV generation current, respectively. $V_{pv\text{rtd}}$ and $V_{sc\text{rtd}}$ are rated voltages of PV generation and supercapacitor, respectively. I_{sc}^* and I_{sc} are reference and measured supercapacitor current, respectively. SW1 and SW2 gate pules for bidirectional DC-DC converter for supercapacitor. Mode control switch is used to shift MPPT control to voltage control mode or vice a versa as per conditions decide. During MPPT control supercapacitor controller also synchronized with battery controller.

3.3 Control of CESS Bidirectional DC-DC Converter

This is the novel approach to control DC bus voltage by composite energy storage system [35]. Li-ion battery supply or receive power of steady state nature whereas supercapacitor supply or receive power of transient nature. Both battery and supercapacitor are interfaced with DC bus via bidirectional DC-DC converter individually. Their control scheme is combined to serve the above-mentioned goal as shown in Fig. 9. In the CESS control loop, reference bus voltage is compared

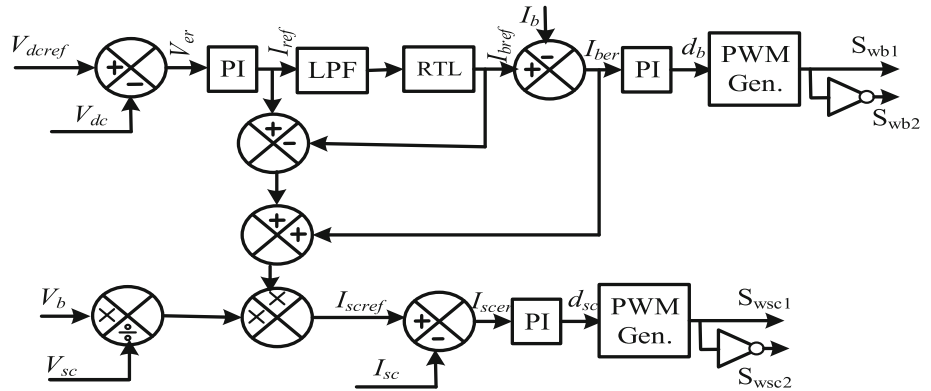
with actual dc bus voltage. The outer voltage PI controller generates the current reference.

Low pass filter (LPF) and rate limiter (RTL) are used to differentiate battery reference current ($I_{b\text{ref}}$) and reference current to be used in supercapacitor controller. The constant power (low frequency) will be handled by battery and transient power (high frequency) by super capacitor. This is implemented to maintain the low stress on battery and thus increase its life. The error component of battery current is also added to the transient current component to manage the uncompensated current for battery as battery converter does not respond instantly to the reference current. The resultant transient reference is nominalized with Battery voltage (Vb) and supercapacitor voltage (Vsc) as explained in Fig. 9. The estimated supercapacitor reference current ($I_{sc\text{ref}}$) is fed to inner current control loop of supercapacitor for transient control in DC bus voltage.

3.4 Various Power Electronics Converters and their Controller Specifications in this Paper

The value of DC-link capacitor (C_{dc}) is calculated by Eq. (6), where P_g , V_{dc} , ΔV_{dc} and ω_1 are the power rating of GSC,

Fig. 9 Combined Control for proposed CESS



DC-link rated voltage, peak to peak ripple content permitted in DC-link voltage and utility grid angular frequency.

$$C_{dc} = \frac{P_g}{V_{dc} \Delta V_{dc} \omega_1} \tag{6}$$

Boost DC-DC converter used for interfacing SPV and DC bus. Its inductor (L_{pv}) and capacitor (C_{pv}) values are calculated by Eq. (7) and (8), respectively [36]. DC-DC Bidirectional converters are used to interface battery and supercapacitor individually. The inductance and capacitance values are decided by Eq. (9–12) [37].

$$L_{pv} = \frac{V_{pv}(V_{bus} - V_{pv})}{\Delta I_L f_{s\omega} V_{bus}} \tag{7}$$

$$C_{pv} = \frac{P_{max} D}{\Delta V_{bus} f_{s\omega} V_{bus}} \tag{8}$$

$$L_b = \frac{V_b D_b}{2 \Delta I_L f_{s\omega}} \tag{9}$$

$$L_{sc} = \frac{V_{sc} D_{sc}}{2 \Delta I_L f_{s\omega}} \tag{10}$$

$$C_b = \frac{V_{bus} D_b}{2 \Delta V_{bus} R_b f_{s\omega}} \tag{11}$$

$$C_{sc} = \frac{V_{bus} D_{sc}}{2 \Delta V_{bus} R_{sc} f_{s\omega}} \tag{12}$$

4 Boost DC-DC Converter Feeding Constant Power Load: Stability Analysis and Mitigation

The constant power load (CPL) which contains a resistor with tightly regulated buck converter. Its V-I characteristics are shown in Fig. 10 with negative incremental resistance. The buck converter is receiving power from 700 V DC bus

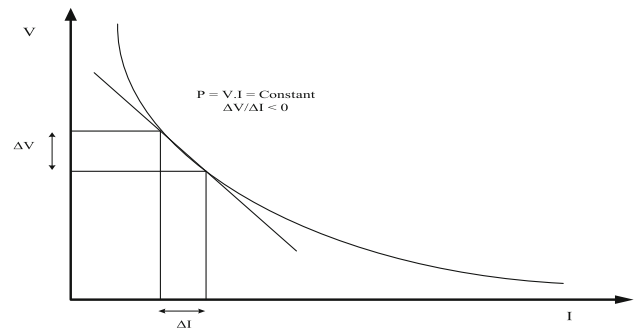


Fig. 10 V-I Characteristics of constant power load

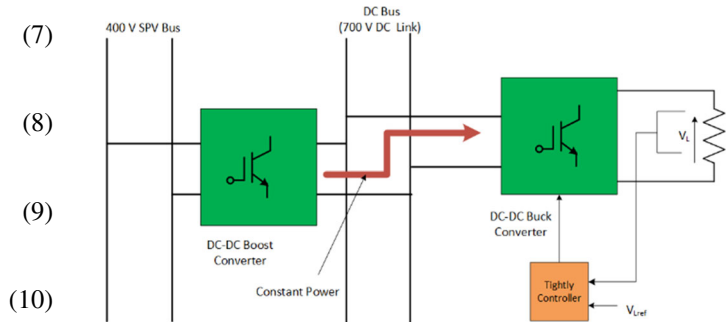


Fig. 11 Constant power load fed by DC- DC boost converter

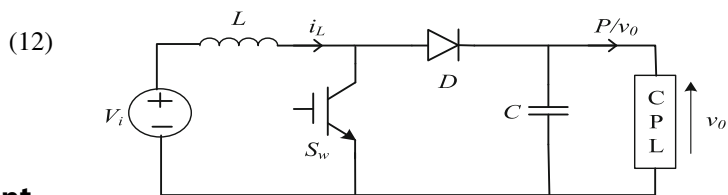


Fig. 12 DC-DC Boost Converter with a Constant Power Load

(PCC) and having duty ratio of 0.4286. This DC bus is receiving power from another upper SPV DC bus of 400 V via boost converter as shown in Fig. 11. The circuit diagram of boost converter with CPL is shown in Fig. 12. The equations of

operation in continuous current mode of DC-DC Boost converter with CPL are given as (13) and (14) [38]. V_i and v_o are input and load voltage, i_L and v_o are state variables. L , C and P is Inductance, capacitance and constant power, respectively. The control output is $u = 1$ for ON and 0 for OFF condition of switch [29].

$$\frac{di_L}{dt} = \frac{1}{L}[V_i - (1 - u)v_o] \quad (13)$$

$$\frac{dv_o}{dt} = \frac{1}{C}\left[(1 - u)i_L - \frac{P}{v_o}\right] \quad (14)$$

Boost converter requires to supply CPL and it also has right hand side zero (RHZ) in its s-domain transfer function. Stability with CPL became a prime concern for operation of boost converter. The Phase portrait of boost converter is given in Fig. 13 to assert its stability behaviors with CPL. For this study the initial value of output capacitor voltage is maintained more than 70 V for stability as it is observed in phase plot. The equilibrium point is maintained at (700 V, 25A) and CPL line passing through this equilibrium as shown in Fig. 13. Separatrix makes boundary between stable and unstable region. Within limit cycle inductor current always has finite value where as in limit region it goes to zero during oscillation.

The controllers for downstream buck as well as upper stream boost converter are designed by double loop control approach as used for battery and supercapacitor interfacing converters. Bode plot technique is used to calculate K_p and K_I constants for controllers. For boost converter, the bode plot is depicted in Fig. 14 with gain margin 9.93 dB and phase margin 104° with $K_p = 0.0612$ and $K_I = 3.845$ for outer

5 Simulation Results and Discussion

5.1 MATLAB/SIMULINK Result

The parameters of proposed grid-connected DCMG are given in Table 1 and it is simulated in MATLAB/SIMULINK environment. The simulation is done for 9 s which is divided based on circumstances/conditions in to four intervals which represent three modes of operation as per flowchart along with utility grid fault. These operating interval/mode and conditions are given in Table 2. Three-phase quantities are presented in per unit for sake of clarity and better understanding. 10 kVA and 400 V are considered base values of power and line voltage, respectively. The utility grid should be healthy to make connection with DCMG. In time interval (0–3 s), utility grid is healthy and a single phasing is created at 0.5 s for 2 s to analyze the effect of supercapacitor on utility grid and DCMG functioning. The simulation results for utility grid side parameters are in pu and presented in Fig. 15

for small duration before and after the fault. Grid voltage is given in Fig. 15a, whereas grid current with single phasing and with supercapacitor is shown in Fig. 15b. It is observed that the current in open circuit phase become zero and, in another phases, have regular pattern with 180° phase utility grid and DCMG, THD of 50.2% and 0.9 pu peak of grid current for given condition. The situation has been reconstituted without supercapacitor and simulated utility grid current is shown in in Fig. 16. It can be found from simulation result that this transition poses threat of stability as well also deteriorate power quality. It is noted that nonzero current phases currents are not of regular pattern, 57% of THD with 1.2 pu peak. These simulation studies clearly manifest utility of supercapacitor in case of severe fault like single phasing difference currents for exchanging power between.

In Fig. 15c, phase-a voltage and respective current are shown, their phase opposition shows that power delivered from DCMG to utility grid. Power electronics converter fed three-phase nonlinear load is connected at PCC, the three-phase load current is shown in Fig. 17 for small duration in steady state condition. DCMG results are presented in Fig. 18 as SPV current, battery current, supercapacitor current, DC critical load current, utility grid current at DC bus, DC bus voltage, battery SoC and Supercapacitor SoC. The various power results and grid status are shown in Fig. 19 as SPV power, battery power, supercapacitor power, DC load power, utility grid power at DC bus, three-phase nonlinear load power, grid power at PCC and grid status with supercapacitor. The simulation is accomplished without supercapacitor and results are presented in Fig. 20. The bus voltage peak to peak ripple during fault is observed as 5.27 V with supercapacitor and 37.95 V without supercapacitor as shown in Fig. 18f and Fig. 20f, respectively. The power surplus mode of operation is simulated for 3 to 6 s interval. During this period, utility grid is unhealthy and battery SoC is unfavorable for CESS mode as explained in flowchart Fig. 2. So, the battery remains idle in this mode and SPV generation shifts from MPPT mode to constant voltage control mode with coordination of supercapacitor. Irradiance is changed from 500 to 700 W/m² at 4.5 s to check the robustness of control. Simulation results of CESS mode are shown in Figs. 18 and 19 for duration 6 to 7.5 s. The DC Bus voltage is controlled by battery and supercapacitor as per the strategy explained in flowchart. No power transaction takes place between DCMG and utility grid. DC-DC Boost converter fed CPL MATLAB/SIMULINK results are shown in Fig. 21.

5.2 Real Time Simulator Results

The OPAL-RT Real-Time Simulator (Opal-RT 4210) is used to validate the MATLAB/SIMULINK result. The validation setup is shown in Fig. 22. The effect of supercapacitor on DC

Fig. 13 Phase portrait of DC-DC boost converter operation for $V_o = 700$ V, $I_L = 25$ A and $D = 0.4286$ with $L_{in} = 6.9$ mH and $C_o = 91.837$ μ F voltage loop. Similarly, for inner current loop, the $K_p = 53.66$ and $K_I = 5257$ are obtained.

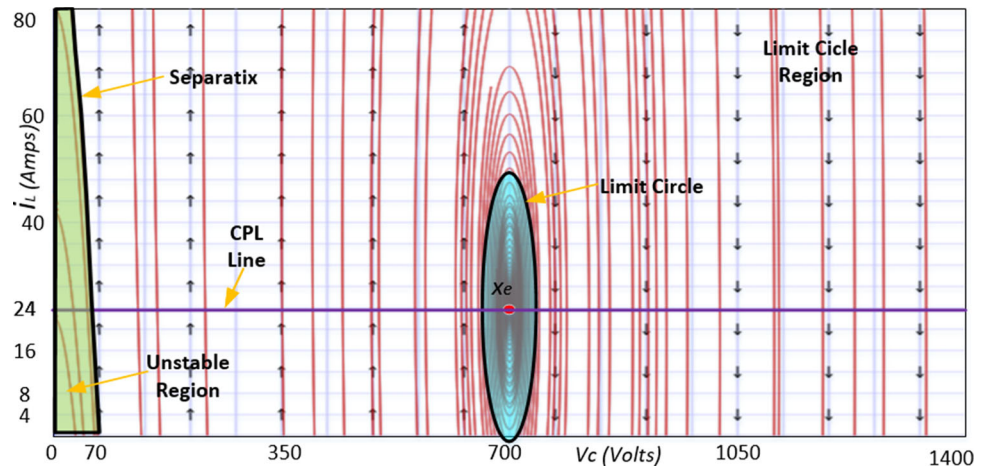


Fig. 14 Bode plot for without controller and with controller of boost converter feeding CPL

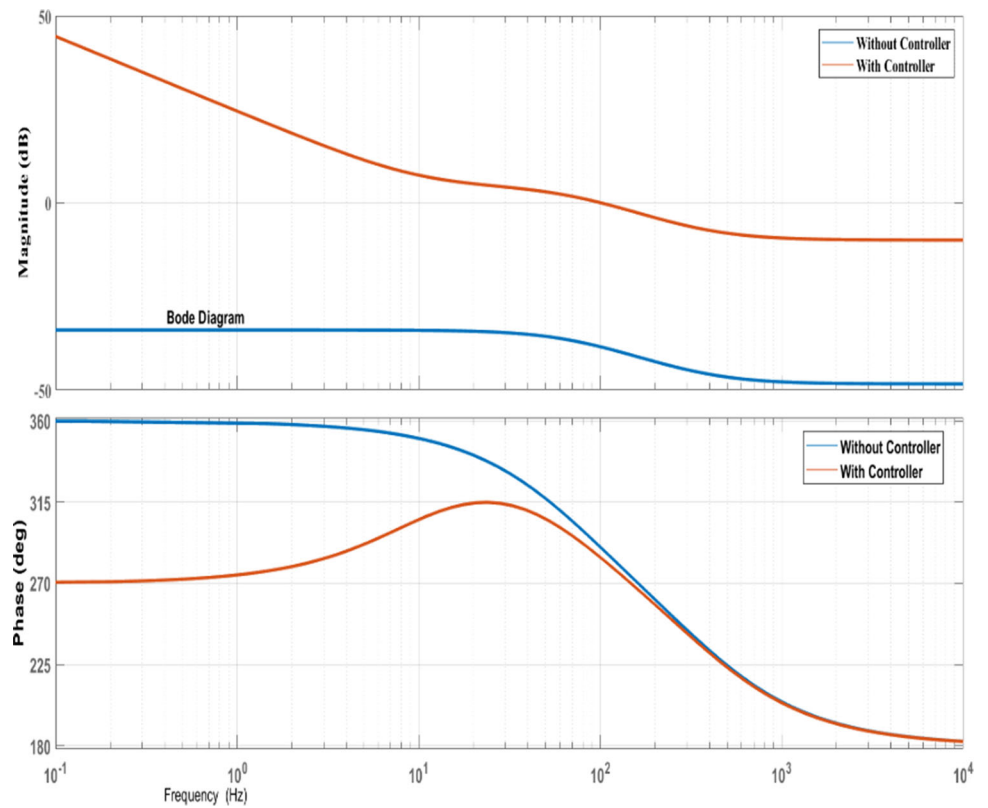


Table 1 Grid-connected DCMG component parameters

Component Name	Specifications
Solar photovoltaic	10kWp,656 V
Li-ion battery	48 V 40Ah, 400 V
Supercapacitor	250F, 300 V
Utility grid	Three-Phase 400 V, 50 Hz,
Critical DC load	10 Kw
Constant power load	10 Kw
Nonlinear three phase- AC load	8 kW,0.995lag., 30.08% THD

bus during utility single phasing verified with OPAL -RT simulation and shown in Fig. 23c6 and Fig. 24c6, respectively. RT-LAB results for CPL are shown in Fig. 25. Response to input disturbances is also observed at 3 s and 6 s which validate the control strategy. Peak to peak ripple in V_{dc} at PCC is observed 21 V whereas input current peak to peak ripple in boost converter is measured as 4A.

Table 2 Grid-connected DCMG operating modes

Operating Modes	Time interval (second)	Irradiance (W/m ²)	Critical DC load (kW)	3 phase nonlinear AC load (kW)	Utility grid status	Battery status (SoC in %, ch/dis/Idle)
ON Grid	0–3	500	8	0	Healthy	10 ≤ SoC ≤ 90 (ch/dis) or Idle
Power surplus mode	3–6	500–700	8	0	Unhealthy	SoC ≤ 30 or 85 ≤ SoC (Idle)
OFF Grid CESS	6–7.5	700	8	0	Unhealthy	30 ≤ SoC ≤ 85 (ch/dis)
ON Grid with NL 3 ph ac load	6–9	700	8	8	Healthy	10 ≤ SoC ≤ 90 (ch/dis) or Idle

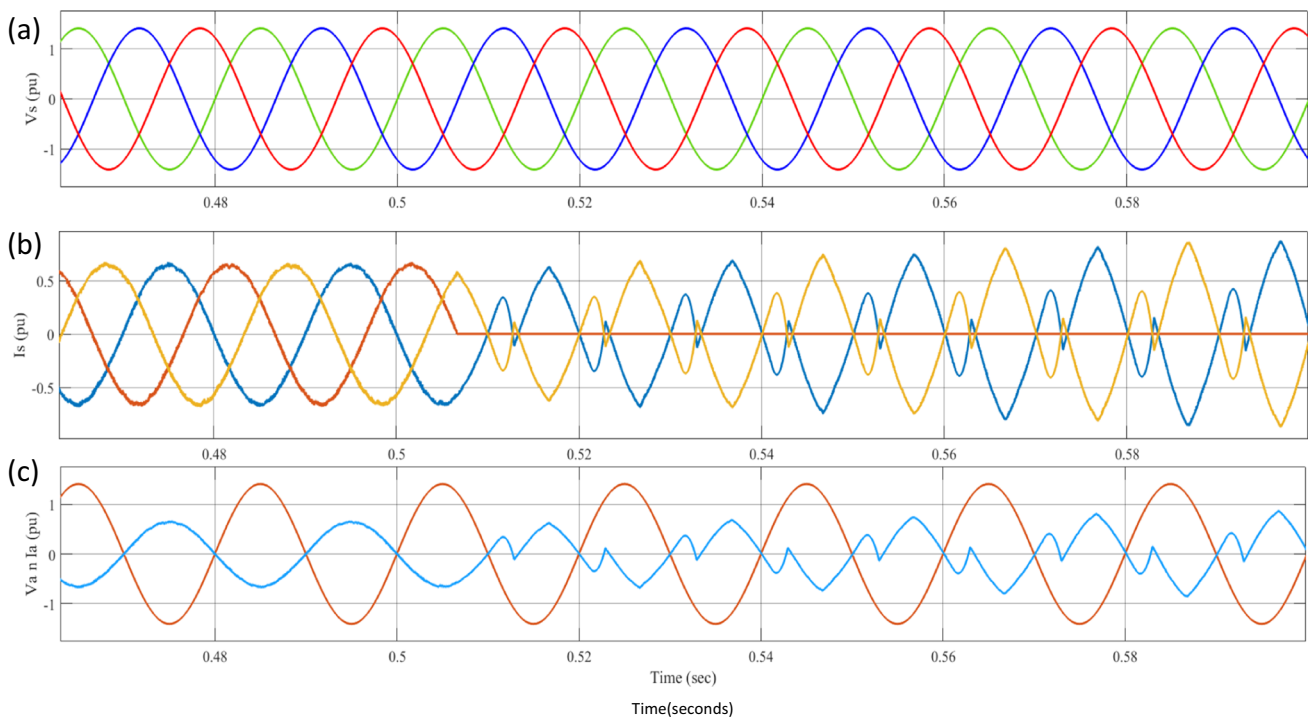


Fig. 15 Utility grid parameters in pu: **a** three-phase grid voltage, **b** three-phase grid current for normal operation and single phasing with supercapacitor (THD = 50.2%), **c** phase-a voltage and respective current

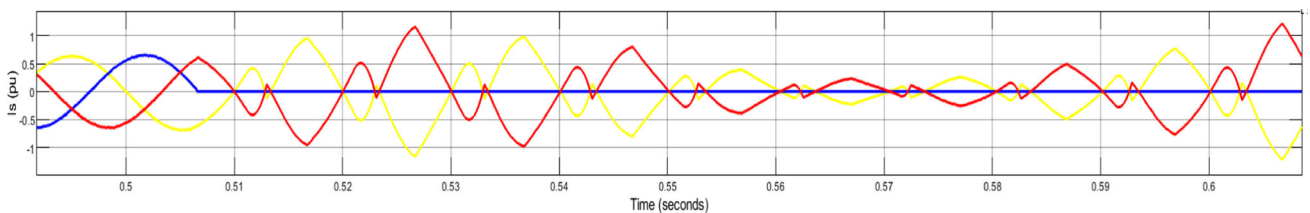


Fig. 16 Three-phase utility grid current for normal operation and single phasing created at 0.5 s without supercapacitor (THD = 57%) during fault

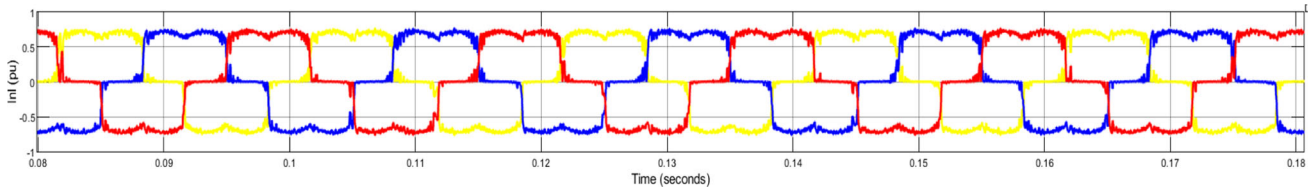


Fig. 17 Three-phase nonlinear load current

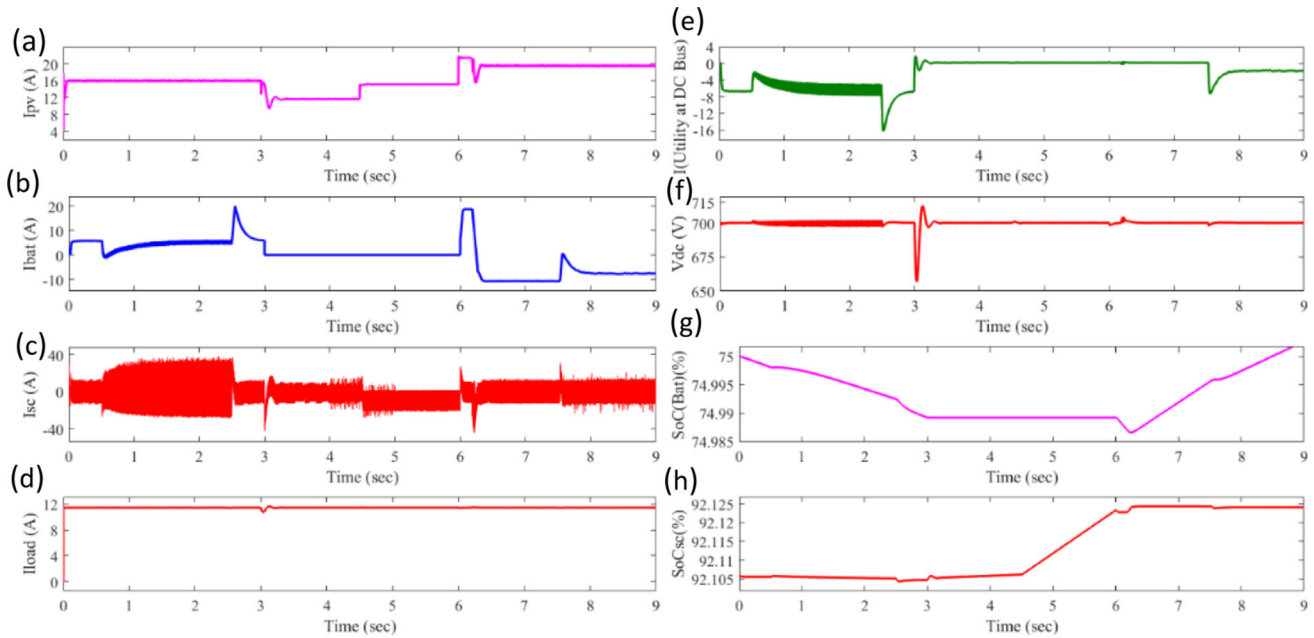


Fig. 18 Proposed system MATLAB/SIMULINK simulation with supercapacitor: **a** SPV current, **b** battery current, **c** supercapacitor current, **d** DC load current, **e** utility grid current at DC bus, **f** DC bus voltage, **g** Battery SoC, **h** Supercapacitor SoC

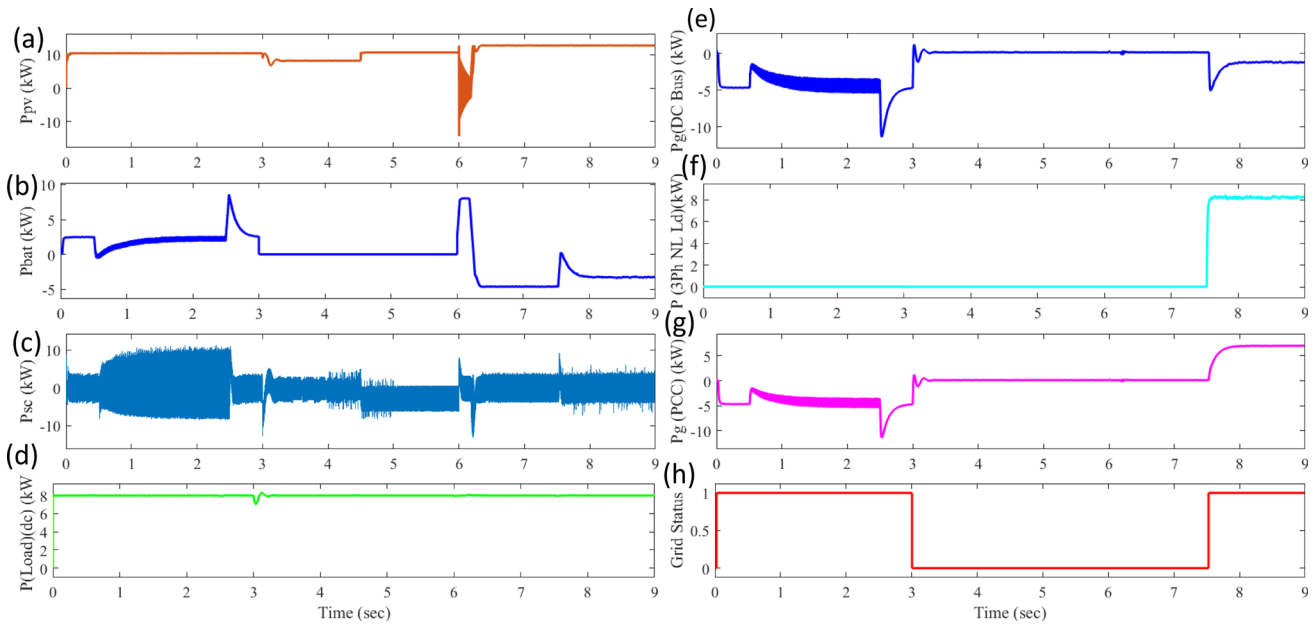


Fig. 19 Proposed system MATLAB/SIMULINK simulation: **a** SPV power, **b** battery power, **c** supercapacitor power, **d** DC load power, **e** utility grid power at DC bus, **f** three-phase nonlinear load power, **g** grid power at PCC, and **h** grid status

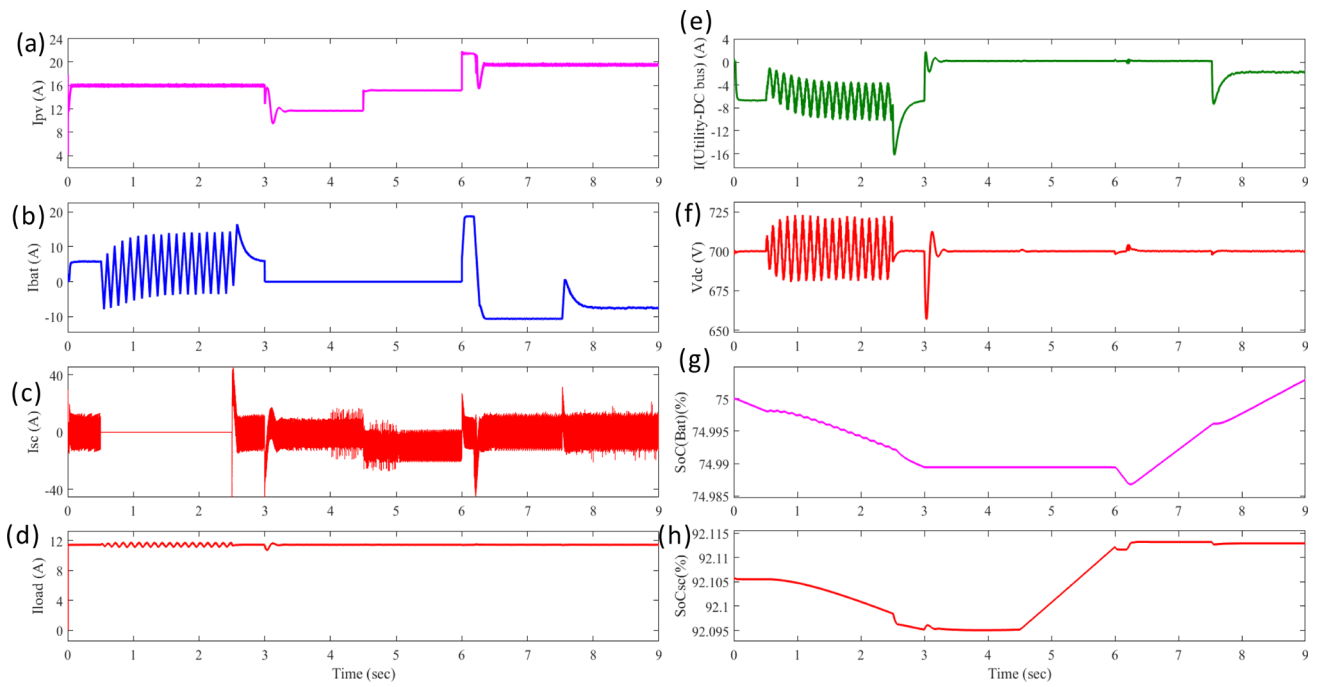


Fig. 20 Proposed system MATLAB/SIMULINK simulation without supercapacitor during fault: **a** SPV current, **b** battery current, **c** supercapacitor current, **d** DC load current, **e** utility grid current at DC bus, **f** DC bus voltage, **g** Battery SoC, **h** Supercapacitor SoC

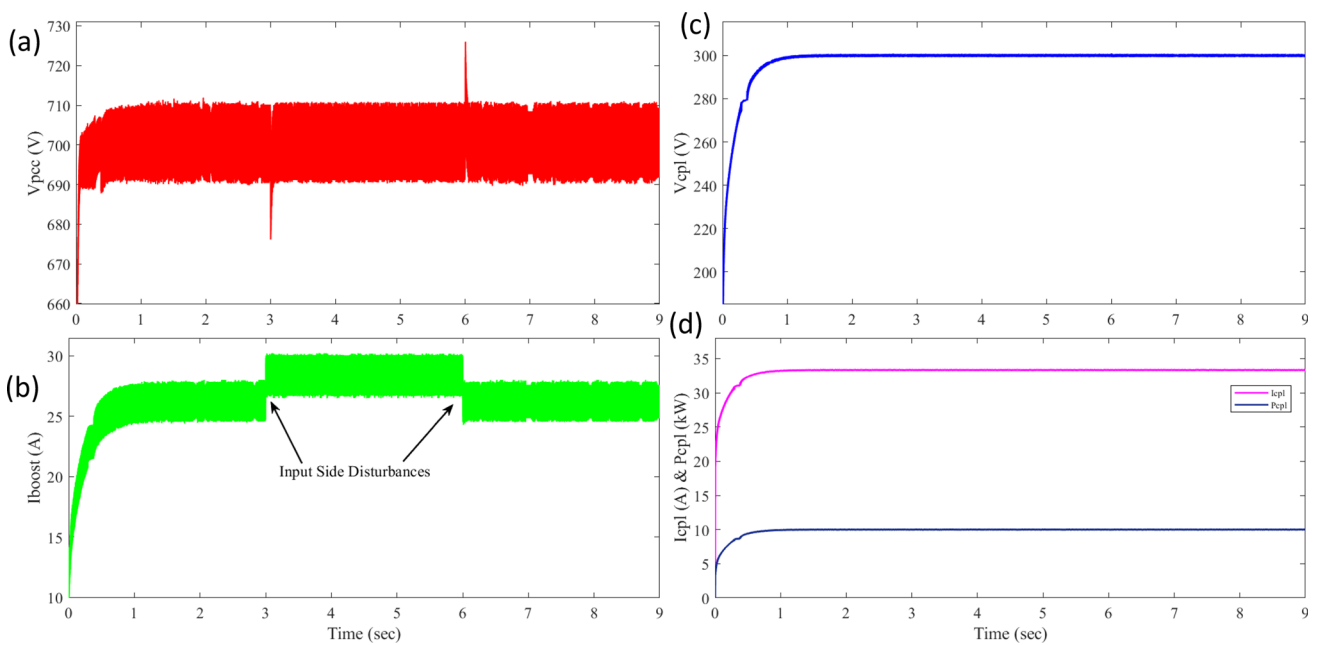


Fig. 21 DC-DC boost converter fed CPL MATLAB/SIMULINK simulation with stability: **a** Vdc at PCC, **b** input current of boost converter, **c** output voltage of CPL, and **d** output current and power of CPL

Fig. 22 OPAL-RT Real Time Simulator: **a** Simulink model for RT Lab, and **b** RT simulator setup picture

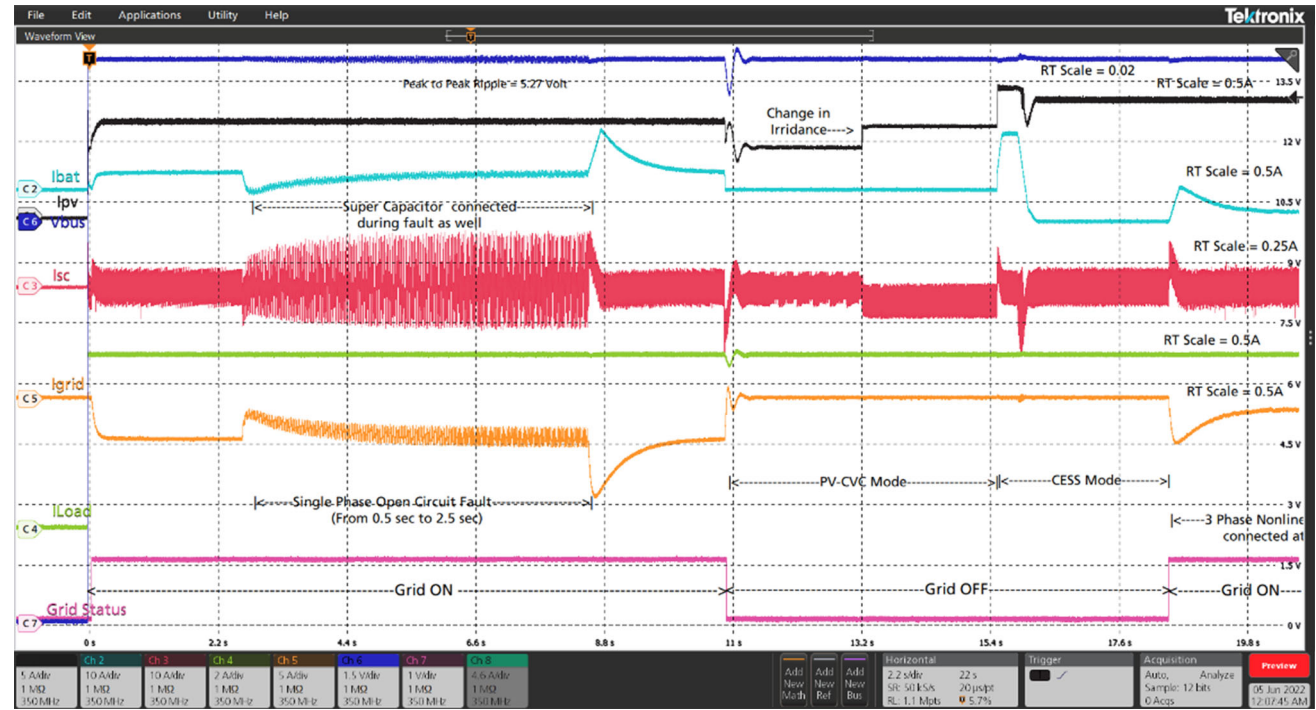
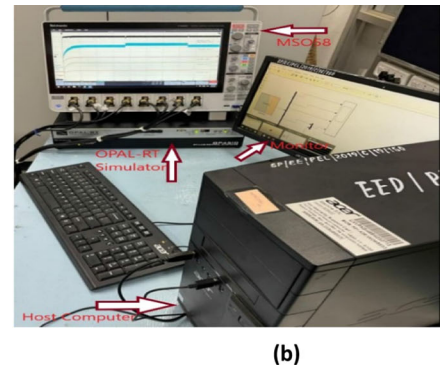
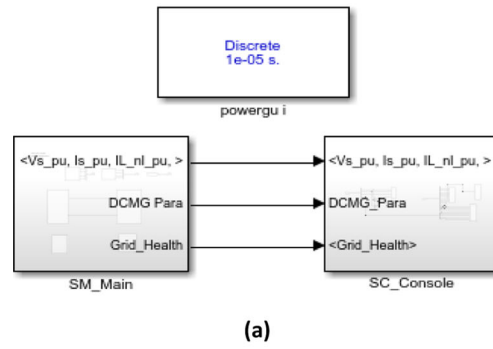


Fig. 23 Real time simulator (Opal-RT) results with supercapacitor: **c1** SPV current, **c2** battery current, **c3** supercapacitor current, **c4** DC load current, **c5** utility grid current at DC bus, **c6** DC bus voltage, and **c7** Grid status

6 Conclusion

In this paper, Utility grid-connected DCMG is simulated in MATLAB/SIMULINK environment for various conditions and modes of operation. The proposed control MATLAB results are validated with OPAL-RT LAB simulator (RT-4210). The system is simulated for ON grid and OFF grid depending on grid health. A single-phase open circuit fault is analyzed with and without super capacitor. The effect of supercapacitor can be seen on ripple at DC bus voltage and pattern of grid current. A three-phase nonlinear load is connected at point of common coupling for utility grid and DCMG. This is partly supplied by Utility grid directly and DCMG by three-phase three-level neutral point

clamped. In OFF grid, power surplus mode and CESS mode are simulated and analyzed. In SPV constant voltage control mode, the DC-DC boost converter shifts its operation from MPPT to CVC with coordination of supercapacitor and battery becomes idle. CESS mode controls the bus voltage and power flow by combined control strategy of battery and supercapacitor controller. Stability issues of DC-DC boost converter fed constant power load as a part of DCMG have been discussed, simulated and validated with Hardware In Loop. Thus, this paper reports the worth of control strategy for CESS-integrated DCMG with On grid and Off grid application.

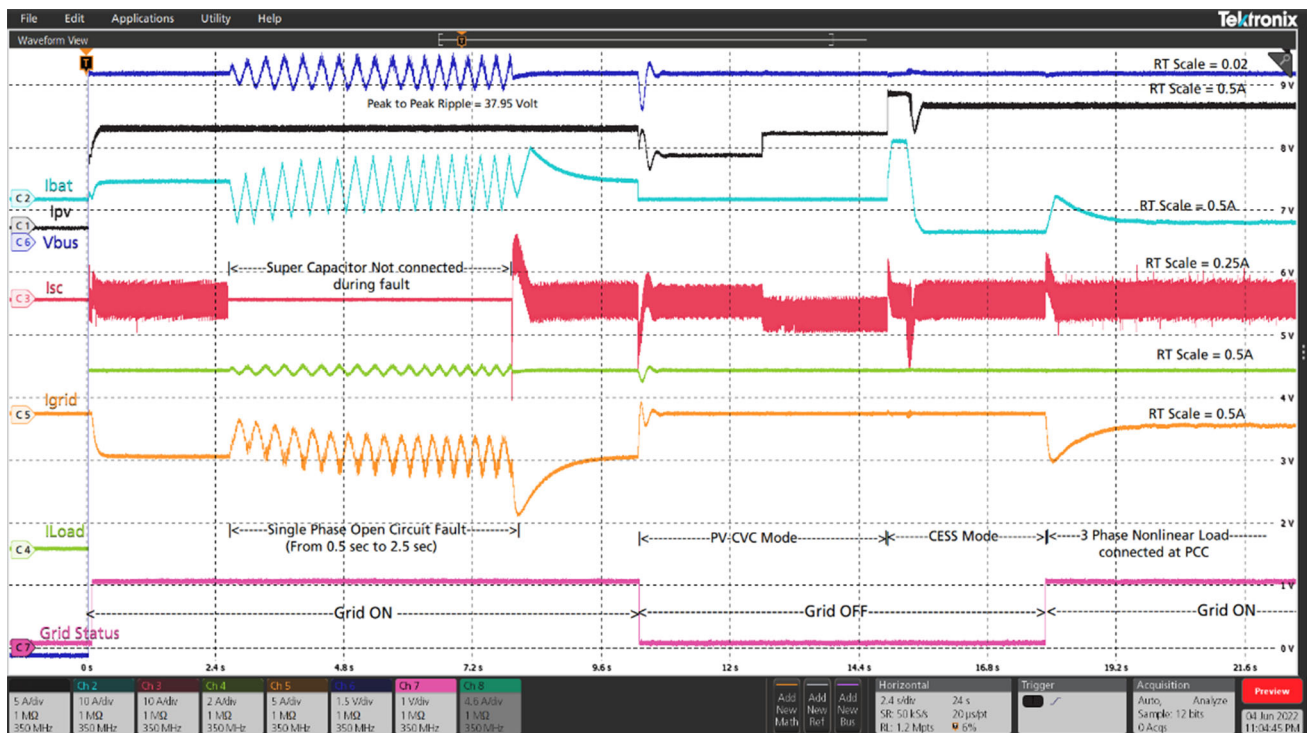
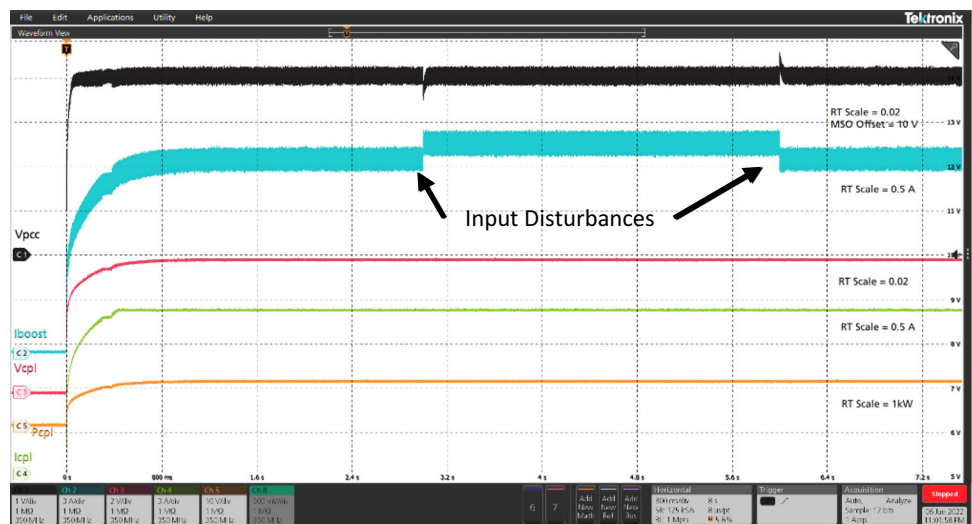


Fig. 24 Real time simulator (Opal-RT) results without supercapacitor (during fault): **c1** SPV current, **c2** battery current, **c3** supercapacitor current, **c4** DC load current, **c5** utility grid current at DC bus, **c6** DC bus voltage, **c7** Grid status

Fig. 25 OPAL-RT Lab Results for boost converter fed CPL with stability: **c1** Vdc at PCC, **c2** input current of boost converter, **c3** output voltage of CPL, **c4** output current of CPL, and **c5** output power of CPL



References

- James, S. M., Momoh, A., Saint, R.: Centralized and Decentralized Generated Power Systems-A Comparison Approach Future Grid Initiative. In: The Future Grid to Enable Sustainable Energy Systems, (2012)
- Dugan, R.C.; McDermott, T.E.: Distributed generation. IEEE Ind. Appl. Mag. **8**(2), 19–25 (2002)
- Ackermann, T.; Andersson, G.; Söder, L.: Distributed generation: a definition. Electric Power Syst. Res. **57**, 195–204 (2001)
- Bird, M. M. L., Lew, D.: Integrating variable renewable energy: challenges and Solutions. National Renewable Energy Laboratory, USA2013.
- Erdiwansyah, M., Husin, H., Nasaruddin, Zaki, Muhibbuddin, M.: A critical review of the integration of renewable energy sources with various technologies. *Protection and Control of Modern Power Systems*, vol. 6, no. 1, p. 3, 2021/02/23 2021.
- Dragičević, T.; Lu, X.; Vasquez, J.C.; Guerrero, J.M.: DC microgrids—part II: a review of power architectures, applications, and standardization issues. IEEE Trans. Power Electron. **31**(5), 3528–3549 (2016)

7. Hirsch, A.; Parag, Y.; Guerrero, J.: Microgrids: A review of technologies, key drivers, and outstanding issues. *Renew. Sustain. Energy Rev.* **90**, 402–411 (2018)
8. Silva, P.; Medeiros, C.M.D.S.: A promising future to DC power system: a review. *IEEE Lat. Am. Trans.* **15**(9), 1639–1642 (2017)
9. Justo, J.; Mwasilu, F.; Lee, J.; Jung, J.-W.: AC-microgrids versus DC-microgrids with distributed energy resources: a review. *Renew. Sustain. Energy Rev.* **24**, 387–405 (2013)
10. Dragičević, T.; Lu, X.; Vasquez, J.C.; Guerrero, J.M.: DC microgrids—part i: a review of control strategies and stabilization techniques. *IEEE Trans. Power Electron.* **31**(7), 4876–4891 (2016)
11. Kumar, D.; Zare, F.; Ghosh, A.: DC microgrid technology: system architectures, AC grid interfaces, grounding schemes, power quality, communication networks, applications, and standardizations aspects. *IEEE Access* **5**, 12230–12256 (2017)
12. Kumar, M.; Srivastava, S.C.; Singh, S.N.: Control strategies of a DC microgrid for grid connected and islanded operations. *IEEE Trans. Smart Grid* **6**(4), 1588–1601 (2015)
13. Amin, M. M.; Elshaer, M. A.; Mohammed, O. A.: DC bus voltage control for PV sources in a DC distribution system infrastructure. In: *IEEE PES General Meeting*, 2010, pp. 1–5.
14. Nasirian, V.; Moayedi, S.; Davoudi, A.; Lewis, F.L.: Distributed cooperative control of DC microgrids. *IEEE Trans. Power Electron.* **30**(4), 2288–2303 (2015)
15. X. Li et al.: Robust and autonomous dc bus voltage control and stability analysis for a dc microgrid. In: *2016 IEEE 8th International Power Electronics and Motion Control Conference (IPEMC-ECCE Asia)*, 2016, pp. 3708–3714.
16. Sharma, R.K.; Mishra, S.: Dynamic power management and control of a PV PEM fuel-cell-based standalone ac/dc microgrid using hybrid energy storage. *IEEE Trans. Ind. Appl.* **54**(1), 526–538 (2018)
17. Tummuru, N.R.; Mishra, M.K.; Srinivas, S.: Dynamic energy management of renewable grid integrated hybrid energy storage system. *IEEE Trans. Industr. Electron.* **62**(12), 7728–7737 (2015)
18. Xu, L.; Chen, D.: Control and operation of a DC microgrid With variable generation and energy storage. *IEEE Trans. Power Delivery* **26**(4), 2513–2522 (2011)
19. Zakzouk, N. E.; Lotfi, R. A.: Power flow control of a hybrid battery/supercapacitor standalone PV system under irradiance and load variations. In: *2020 10th International Conference on Power and Energy Systems (ICPES)*, 2020, pp. 469–474.
20. Kollimalla, S.K.; Mishra, M.K.; Ukil, A.; Gooi, H.B.: DC grid voltage regulation using new HESS control strategy. *IEEE Trans. Sustain. Energy* **8**(2), 772–781 (2017)
21. Kotra, S.; Mishra, M.K.; Chaithanya, N.P.: “Design and small signal analysis of DC microgrid with hybrid energy storage system,” in: *IEEE PES Asia-Pacific Power and Energy Eng. Conf. (APPEEC)* **2017**, 1–6 (2017)
22. Ensermu, G.; Bhattacharya, A.; Panigrahy, N.: Real-time simulation of smart DC microgrid with decentralized control system under source disturbances. *Arabian J. Sci. Eng.* **44**, 7173–7185 (2019)
23. Augustine, S.; Mishra, M. K.; Narasamma, N. L.: Proportional droop index algorithm for load sharing in DC microgrid. In: *2014 IEEE International Conference on Power Electronics, Drives and Energy Systems (PEDES)*, 2014, pp. 1–6.
24. Narsa Reddy Tummuru, M. K. M.; Srinivas, S.: Dynamic energy management of renewable grid integrated hybrid energy storage system. *IEEE TRANSACTIONS ON INDUSTRIAL ELECTRONICS*, vol. VOL. 62, , no. DECEMBER 2015, p. 10, 2015.
25. Al-Nussairi, M.; Bayindir, R.; Sanjeevikumar, P.; Mihet-Popa, L.; Siano, P.: Constant power loads (CPL) with microgrids: problem definition, stability analysis and compensation techniques. *Energies*, vol. 10, 10/19 2017.
26. Kwasinski, A.; Onwuchekwa, C.N.: Dynamic behavior and stabilization of DC microgrids with instantaneous constant-power loads. *IEEE Trans. Power Electron.* **26**(3), 822–834 (2011)
27. Shafiee, Q.; Dragicevic, T.; Vasquez, J.C.; Guerrero, J.M.: “Modeling, stability analysis and active stabilization of multiple DC-microgrid clusters. *IEEE Int. Energy Conf. (ENERGYCON)* **2014**, 1284–1290 (2014)
28. Kumar, R.; Sneha, S.; Behera, R. K.: Controller gain impact on islanded dc microgrid stability with constant power load. In: *2018 IEEE International Conference on Power Electronics, Drives and Energy Systems (PEDES)*, 2018, pp. 1–6.
29. Al-Nussairi, M. K.; Bayindir, R.: DC-DC boost converter stability with constant power load. In: *2018 IEEE 18th International Power Electronics and Motion Control Conference (PEMC)*, 2018, pp. 1061–1066.
30. Li, X., et al.: Flexible interlinking and coordinated power control of multiple DC microgrids clusters. *IEEE Trans. Sustain. Energy* **9**(2), 904–915 (2018)
31. Pillay, T.L.; Saha, A.K.: “A comparative analysis of a three phase neutral point clamped multilevel inverter. *IEEE PES/IAS Power-Africa* **2018**, 232–237 (2018)
32. Kesler, M.; Ozdemir, E.: Synchronous-reference-frame-based control method for UPQC under unbalanced and distorted load conditions. *IEEE Trans. Industr. Electron.* **58**(9), 3967–3975 (2011)
33. Geddada, N.; Karanki, S. B.; Mishra, M. K. J. I. I. C. o. P. E.: Drives, E. Systems, Synchronous reference frame based current controller with SPWM switching strategy for DSTATCOM applications,” pp. 1–6, 2012.
34. Soreng, B.; Garnayak, R.; Pradhan, R.: A synchronous reference frame based pll control for a grid-tied photovoltaic system. In: *2017 International Conference on Current Trends in Computer, Electrical, Electronics and Communication (CTCEEC)*, 2017, pp. 1017–1022.
35. Augustine, S.; Mishra, M.K.; Lakshminarasamma, N.: A unified control scheme for a standalone solar-PV low voltage DC Microgrid system with HESS. *IEEE J. Emerg. Selected Topics in Power Electron.* **8**(2), 1351–1360 (2020)
36. B. H. “Basic Calculation of a Boost Converter’s Power Stage, *Texas Instruments Incorporated, Application Report*, , vol. SLVA372C–November 2009–Revised January 2014, p. 9, 2014.
37. Chao, K.H.; Ming-Chang, T.; Chun-Hao, H.; Liu, Y.G.; Huang, L. C.: Design and implementation of a bidirectional DC-DC converter for stand-alone photovoltaic systems. *International Journal of Computer, Consumer and Control (IJ3C)*, , paper vol. Vol. 2, no. (2013), p. 12, 2013.
38. Erickson, R. W.: *Fundamentals of power electronics*, no. Second Edition, 2004. Kluwer Academic Publishers New York, Boston, Dordrecht, London, Moscow

Springer Nature or its licensor (e.g. a society or other partner) holds exclusive rights to this article under a publishing agreement with the author(s) or other rightsholder(s); author self-archiving of the accepted manuscript version of this article is solely governed by the terms of such publishing agreement and applicable law.